Article

Protrusive and Contractile Forces of Spreading Human Neutrophils

Steven J. Henry,[1] Christopher S. Chen,[2] John C. Crocker,[3,*] and Daniel A. Hammer[1,3,*]
[1]Bioengineering, University of Pennsylvania, Philadelphia, Pennsylvania; [2]Biomedical Engineering, Boston University, Boston, Massachusetts; and [3]Chemical and Biomolecular Engineering, University of Pennsylvania, Philadelphia, Pennsylvania

ABSTRACT Human neutrophils are mediators of innate immunity and undergo dramatic shape changes at all stages of their functional life cycle. In this work, we quantified the forces associated with a neutrophil's morphological transition from a nonadherent, quiescent sphere to its adherent and spread state. We did this by tracking, with high spatial and temporal resolution, the cell's mechanical behavior during spreading on microfabricated post-array detectors printed with the extracellular matrix protein fibronectin. Two dominant mechanical regimes were observed: transient protrusion and steady-state contraction. During spreading, a wave of protrusive force (75 ± 8 pN/post) propagates radially outward from the cell center at a speed of 206 ± 28 nm/s. Once completed, the cells enter a sustained contractile state. Although post engagement during contraction was continuously varying, posts within the core of the contact zone were less contractile (−20 ± 10 pN/post) than those residing at the geometric perimeter (−106 ± 10 pN/post). The magnitude of the protrusive force was found to be unchanged in response to cytoskeletal inhibitors of lamellipodium formation and myosin II-mediated contractility. However, cytochalasin B, known to reduce cortical tension in neutrophils, slowed spreading velocity (61 ± 37 nm/s) without significantly reducing protrusive force. Relaxation of the actin cortical shell was a prerequisite for spreading on post arrays as demonstrated by stiffening in response to jasplakinolide and the abrogation of spreading. ROCK and myosin II inhibition reduced long-term contractility. Function blocking antibody studies revealed haptokinetic spreading was induced by β_2 integrin ligation. Neutrophils were found to moderately invaginate the post arrays to a depth of ~1 μm as measured from spinning disk confocal microscopy. Our work suggests a competition of adhesion energy, cortical tension, and the relaxation of cortical tension is at play at the onset of neutrophil spreading.

INTRODUCTION

Neutrophils are white blood cells of the innate immune system. They act as first responders to tissue trauma (1) and pathogen challenges (2), initiating the body's inflammatory response on the timescale of seconds to minutes. Central to neutrophil function is spreading in which the cell begins as a quiescent sphere and becomes well spread and migratory (3). There are numerous observations of the dynamics of neutrophil spreading in vitro. Lomakina et al. (4) measured neutrophil spreading as haptokinetic stimulation by immobilized fields of the chemokine interleukin 8. Sengupta et al. (5) measured neutrophil spreading on continuous fields of fibronectin (FN), induced by soluble formylated chemotactic peptide. Using reflection interference contrast microscopy (RICM), they observed that regions of closest membrane contact to the substrate were present at the periphery of the spreading cell. It was hypothesized that these regions would ultimately correspond to domains of high force generation. In neither study were the tractions associated with neutrophil spreading directly measured.

Our goal in this work was to measure the forces of neutrophil spreading on microfabricated post-array detectors (mPADs). Although mPADs have long been used to measure forces in mesenchymal cells (6–10), they have only recently been employed to study immune cell function. Ricart et al. (11) used mPADs to measure the traction stresses of dendritic cells undergoing chemotaxis and established that these cells migrate by a frontward pulling mechanism. Bashour et al. (12) explored the mechanics of T-lymphocyte activation and spreading on mPADs functionalized by antibodies to the activation receptors CD28 and CD3. Although the mechanodynamics of T-lymphocyte spreading were measured, the role of the cell cytoskeleton was not investigated.

Here, we report the protrusive and contractile behavior of spreading neutrophils with high spatial and temporal resolution on FN printed mPADs. Spreading was a fast, radially symmetric wave sufficiently forceful to generate outward deflections of the underlying posts. After protrusion, cells contracted with posts on the perimeter of the contact zone exhibiting higher contractility than those in the core. Small molecule inhibitor perturbations of the cellular cytoskeleton revealed that cortical actin relaxation was critical upstream of protrusion but protrusion itself was not myosin II dependent. Conversely, long-term sustained contractility was dependent on ROCK and myosin II. Function blocking antibody studies revealed that haptokinetic spreading on FN was β_2 integrin induced. Confocal z-stacks uncovered moderate post invagination into the cell body, which was ultimately

Submitted January 23, 2015, and accepted for publication May 26, 2015.
*Correspondence: jcrocker@seas.upenn.edu or hammer@seas.upenn.edu
Editor: David Odde.

0006-3495/15/08/0699/11
http://dx.doi.org/10.1016/j.bpj.2015.05.041

fortuitous in reporting the energy associated with the quiescent-to-spread shape change.

MATERIALS AND METHODS

Media and reagents

Details are provided in the Supporting Material.

mPADs and microcontact printing

mPADs were fabricated and printed as detailed by Yang et al. (13). Details are provided in the Supporting Material. Scanning electron microscopy of our cast arrays (Fig. 1 *A*) allowed us to characterize the post geometry (diameter = 604 ± 31 nm, length = 5.576 ± 0.286 μm, m ± SD) and compute an associated spring constant, $k_{spring} = 0.28 \pm 0.09$ pN/nm. For these posts, with length ten-fold longer than width, Schoen et al. (14) showed that the substrate warping correction to k_{spring} was 8%. This correction was less than the measurement error in k_{spring} for our experiments. Details of the calculation of the spring constant and the Schoen et al. correction are provided in the Supporting Material.

Neutrophil isolation

Blood was collected with University of Pennsylvania Institutional Review Board approval from consenting adult volunteers. Cells were isolated as previously described (15). Details are provided in the Supporting Material.

Spreading experiments

Brightfield and fluorescence microscopy were performed using a spinning disk confocal mounted on an Olympus IX71 base in the University of Pennsylvania's Cell and Developmental Biology Microscopy Core facility. Before cell plating, the experimental chamber was mounted on a 37°C temperature-controlled stage. Images were acquired with a 60× water immersion lens at a frame rate of 1 frame/s. Acquisition began before cell plating. A small volume of suspended neutrophils were introduced into the experimental chamber and allowed to gravity sediment onto the FN printed mPADs.

Antibody blocking and cytoskeletal inhibitor studies

To assess the role of β_2 integrins in neutrophil spreading and adhesion on post arrays, quiescent neutrophils were incubated for 30 min at 4°C on a tube inverter with anti-β_2 clone L130 (BD Biosciences, Franklin Lakes, NJ) at 50 μg/mL. This clone and concentration were previously shown by us (15) and others (16) to be a functional blocking antibody of neutrophil adhesion on FN. To assess the roles of various cytoskeletal components during spreading, quiescent neutrophils were incubated for 30 min at 4°C on a tube inverter with the small molecule inhibitor at the stated final concentration. The corresponding experimental chamber was pretreated at 37°C for 30 min with the same inhibitor concentration. The small molecule inhibitors explored, having previously been demonstrated to alter hematopoietic cell mechanics, were: 5 μM blebbistatin (Sigma-Aldrich, St. Louis, MO) (17), 1 μM CK666 (Sigma-Aldrich, Lot: 043M4606V) (18), 3 μM cytochalasin B (Sigma-Aldrich) (19), 1 μM jasplakinolide (Life Technologies, Frederick, MD) (17,20), and 1 μM Y27632 (EMD Millipore, Billerica, MA) (21).

Cell profile imaging

To map the neutrophil vertical profile during spreading, cell membranes were stained with the lipophilic dye delta9-DiI (DiI) at a final concentration of 50 ng/mL for 15 min on a tube inverter at 4°C. Cells were rinsed twice with fresh storage buffer by gentle centrifugation at 200 × *g* for 5 min. Z-slices were acquired at 0.25 μm intervals. For membrane staining experiments, posts were labeled with AlexaFluor-488 conjugated FN (FN-AF488) only, not DiI.

Data analysis

Fluorescence image stacks focused on the plane of post tips were processed via a series of custom MATLAB (The MathWorks, Natick, MA) scripts. These scripts identified fluorescently labeled post centroids, connected centroids in consecutive frames to form trajectories, subtracted drift from the trajectories, and positioned them relative to their undeflected resting lattice locations. Aspects of our scripts were adapted from the publicly available MATLAB routines (22) of Pelletier et al. (23), which were based upon Crocker and Grier's original particle tracking code (24).

RESULTS AND DISCUSSION

Neutrophil spreading on mPADs

Quiescent neutrophils were capable of spreading atop a plane of FN printed post tips. The onset of spreading was concomitant with strong outward deflections observed at a few posts in the center of the final contact zone and propagated in a radially symmetric wave until the cell's final and maximum spread area was reached (Fig. 1 *B*). This transient protrusive signature was replaced by a sustained contractile phase a few minutes after spreading ceased. The complete spreading sequence with superimposed deflection vectors of Fig. 1 *B* is provided in Movie S1. Post positions were tracked in the fluorescence channel as cell lensing obscured tip detection under brightfield microscopy. Cell-engaged posts experienced significant deflections compared to their nonengaged counterparts (Fig. 1 *C*). This fact was exploited to filter cell-engaged from nonengaged posts in the field of view by considering the variance of the trajectories (Fig. S1). The enlargement of a single perimeter post (Fig. 1 *D*) reveals a strong radial bias in the post's motion away from and toward the center of the cell's final contact zone.

From post deflections, we quantified force trajectories in the cell reference frame in the radial and tangential directions (Fig. S2). For each post, a force trajectory was constructed by multiplying the deflection from the resting lattice position with the known spring constant of the posts ($k_{spring} = 0.28 \pm 0.09$ pN/nm). The noise in the force detection for our system was 9 ± 2 pN as determined by calculation of the mean displacement of posts not contacted by the cell and multiplication by the spring constant. At maximum cell-generated protrusion and contraction this detection threshold resulted in signal/noise ratios of 8:1 and 12:1, respectively.

When we compared an ensemble plot of the radial force of each post between the periphery and the core as a function of time (*gray lines*, Fig. 2 *B*), a clear stratification of the data occurred. By mapping the deflection trajectories

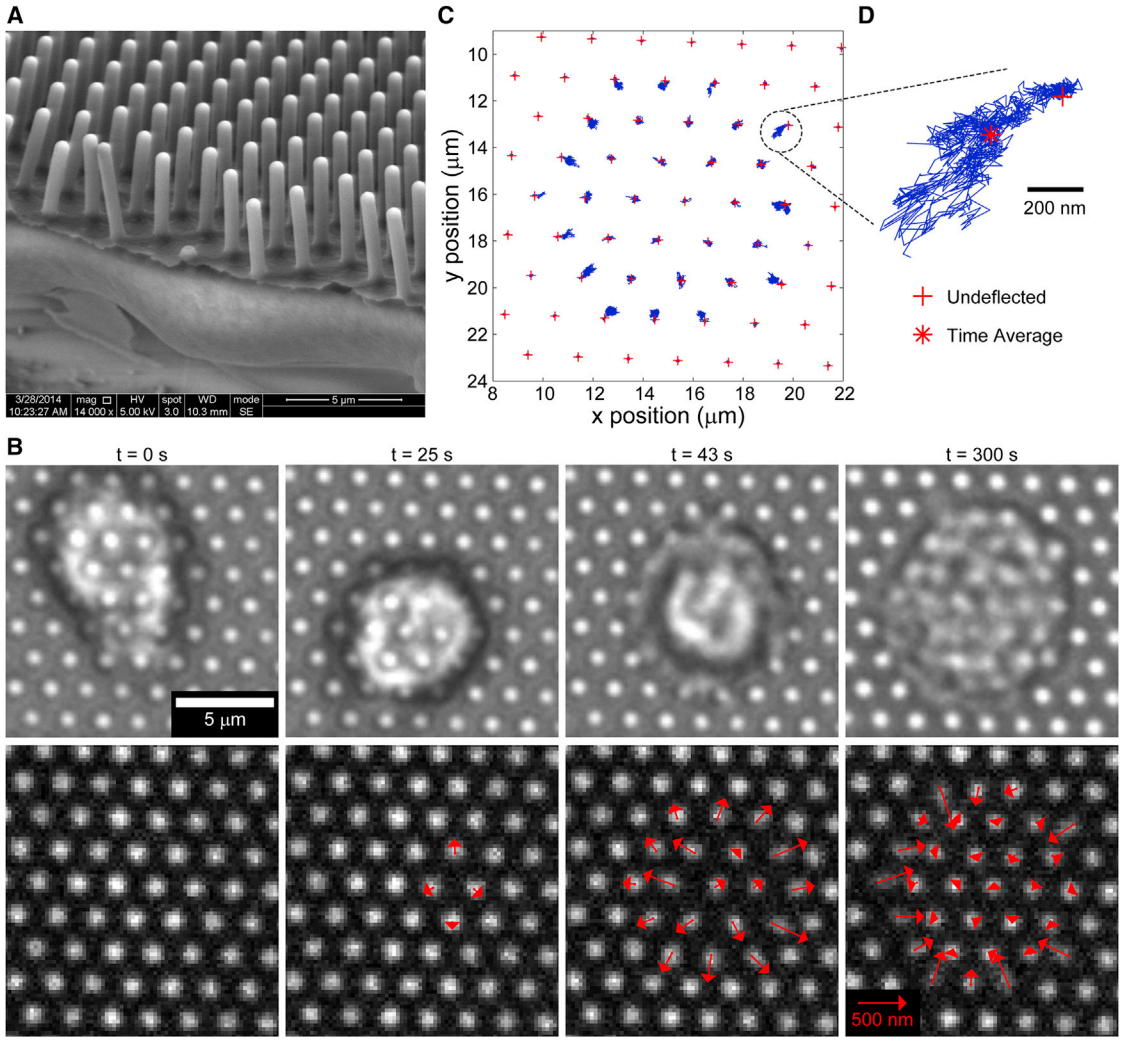

FIGURE 1 Human neutrophil spreading on FN printed mPADs. (*A*) Scanning electron microscopy image of mPADs used in this study. (*B*, *top row*) Bright-field frames from time-lapse sequence of a single neutrophil rapidly spreading across an array of posts. (*B*, *bottom row*) Corresponding frames in fluorescence channel of post tips with superimposed deflection vectors (enlarged 5× to aid visualization). Frames were taken from the full time-lapse sequence provided in Movie S1. (*C*) Trajectories of each post in (*B*) as recorded for 25 min. Red cross-hairs denote the resting lattice position of the undeflected posts. The dotted circle is the enlarged post trajectory of (*D*), where the red asterisk marks the time average position of the trajectory.

of posts within the top (*low contractility*) and bottom (*high contractility*) bands to the spatial position of the posts in the contact zone, two groups of posts emerged. Perimeter posts were generally strongly contractile at long times as compared to core posts. However, both sets exhibited a strong transient protrusive spike. The ensemble averages of Fig. 2 *B* show two major mechanical regimes: initial transient protrusion and long sustained contraction. Although tangential deflections were present throughout the experiment, no net asymmetry in the form of cell rotation or twist was observed (Fig. 2 *C*).

Metrics of spreading and contractility

The behavior of the single spreading neutrophil illustrated in Figs. 1 and 2 and Movie S1 is representative of our entire set of observations of neutrophils spreading under control conditions ($n = 14$ cells, 4 different donors, 386 post trajectories) as shown in Fig. 3 *A*. Whereas in Fig. 2 *B* the mean curves were of the ensemble of posts beneath a single cell, in Fig. 3 A the mean curves are of the ensemble of all mean trajectories for our entire set of 14 spreading cells. To achieve this mean of means, the independent mean radial trajectories were aligned on their respective protrusive maxima and assigned the elapsed event time $\tau = 0$.

The qualitative and quantitative similarity of the protrusive event for core and perimeter posts is evident in the expanded view of Fig. 3 *B* in which the forcefulness and duration of the protrusive events are similar. Protrusion was immediately followed by a contractile rebound. Outwardly deflected posts did not settle back to their resting lattice position but were summarily deflected inward. In the

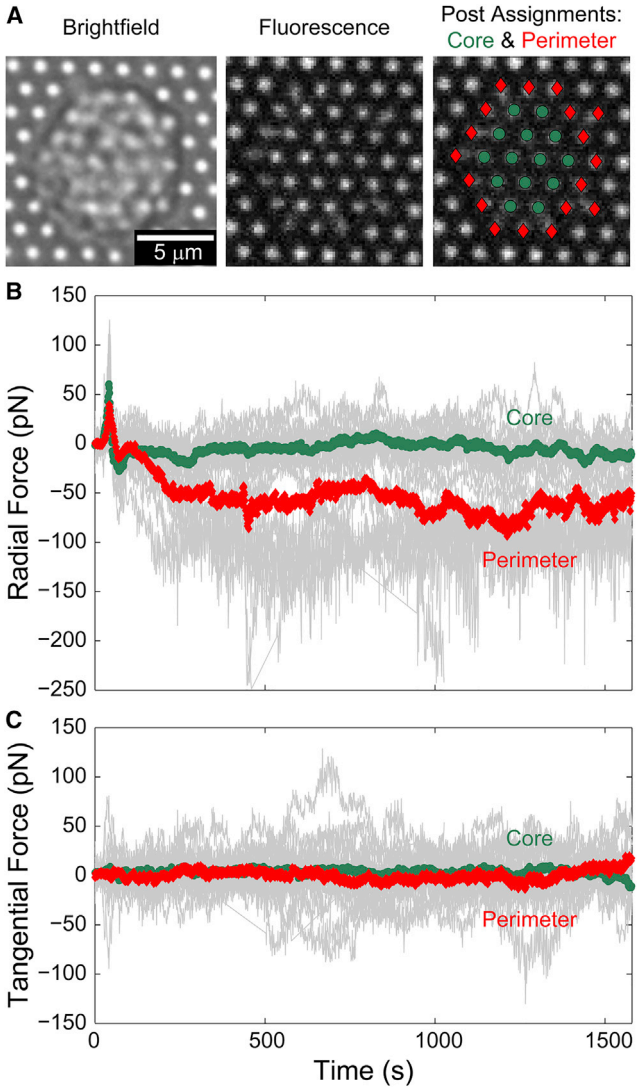

FIGURE 2 Dichotomization of force trajectories. (*A*) Brightfield and fluorescence channel frames at $t = 300$ s from Fig. 1 *B*. Green circles and red diamonds denote the subset of posts residing in the core and at the perimeter of the contact zone, respectively. (*B*) Radial force trajectories over time. (*C*) Tangential force trajectories over time. In (*B*) and (*C*), individual gray lines correspond to individual cell-engaged posts. Ensemble averages of the subset of perimeter (*red diamonds*) and core (*green circles*) posts are superimposed.

core of the cell, the rebound resulted in a transient contractile maximum that relaxed to a less contractile steady state. However, in the perimeter, the posts continuously deflected to a steady-state contractile maximum.

To better capture the wave-like propagation of the protrusive front during spreading, we plotted the time at which protrusive force was a maximum as a function of the radial distance of the protrusive event from the cell centroid for each cell and fit the data with a linear equation. The inverse of the best-fit slope was the cell's spreading velocity. Fig. 3 *C* shows the ensemble best-fit equation for all spreading events (all per-cell fits are reported in Fig. S3). Using this analysis we computed a mean neutrophil spreading velocity of 206 ± 28 nm/s (m ± SE).

We considered a variety of metrics to characterize the radial forces during the transient protrusive (Fig. 3 *D*) and steady-state contractile (Fig. 3 *E*) regimes. Consistent with our qualitative observations, the protrusive signatures of core and perimeter posts were not significantly different with respect to the maximum force generated (~75 pN) (Fig. 3 *D*, *i*), duration of the protrusive deflection (full width at half-maximum (FWHM) ~17 s) (Fig. 3 *D*, *ii*) or the variance in the ensemble of maximum forces (~24 pN^2) (Fig. 3 *D*, *iii*). We did however find a significant decrease in the fraction of perimeter posts (perim: 0.67 ± 0.05) that exhibited a protrusive spike as compared to the fraction of core posts (core: 0.83 ± 0.05) (Fig. 3 *D*, *iv*). Thus, during spreading, when a post was protrusively engaged by the cell, the basic dynamic form of the deflection did not depend on whether the post was at the core or the periphery. However, as distance from the cell centroid increased the occurrence of protrusion decreased.

Within the steady-state contractile regime we found significant differences in core and perimeter posts with respect to the sustained contractile force (core: −20 ± 10 vs. perim: −106 ± 10 pN/post) and its variance (core: 16 ± 4 vs. perim: 46 ± 4 pN^2/post). Perimeter posts were five times more contractile (Fig. 3 E, *i*) and had three times greater variability (i.e., larger distributions in force) in their sustained contractility (Fig. 3 *E*, *ii*) compared to their core counterparts. Our observation that spread neutrophils were most contractile at their periphery compliments the RICM measurements of spreading neutrophils on FN by Sengupta et al. (5). In that prior work, the region of intimate membrane-substrate contact was located at the periphery of the spreading neutrophil. It was hypothesized there, and experimentally demonstrated here, that those regions of intimate membrane-substrate contact are concurrently regions of greatest force generation.

Contrasting our work with Bashour et al. (12), we see greater protrusive and contractile behavior of spreading neutrophils as compared to T-lymphocytes. Spreading neutrophils were approximately sixfold more protrusive and twofold more contractile than activated T-lymphocytes. Bashour and coworkers describe a transient regime between spreading and steady-state contraction in their data in which T-lymphocyte tractions were highly uncoordinated. In our data, we do not see a latent period of uncoordinated traction. Rather, we observe outward protrusion immediately followed by an inward contractile rebound. At the perimeter, this rebound evolves into a highly contractile steady state. The experiments of Bashour et al. measured the mechanics associated with T-lymphocyte activation through the CD3 T cell receptor and the CD28 co-receptor. Ligation of these receptors induces cytoskeletal rearrangement but is upstream of integrin activation, representing an inside-out pathway. Although the mechanism of inside-out T-cell

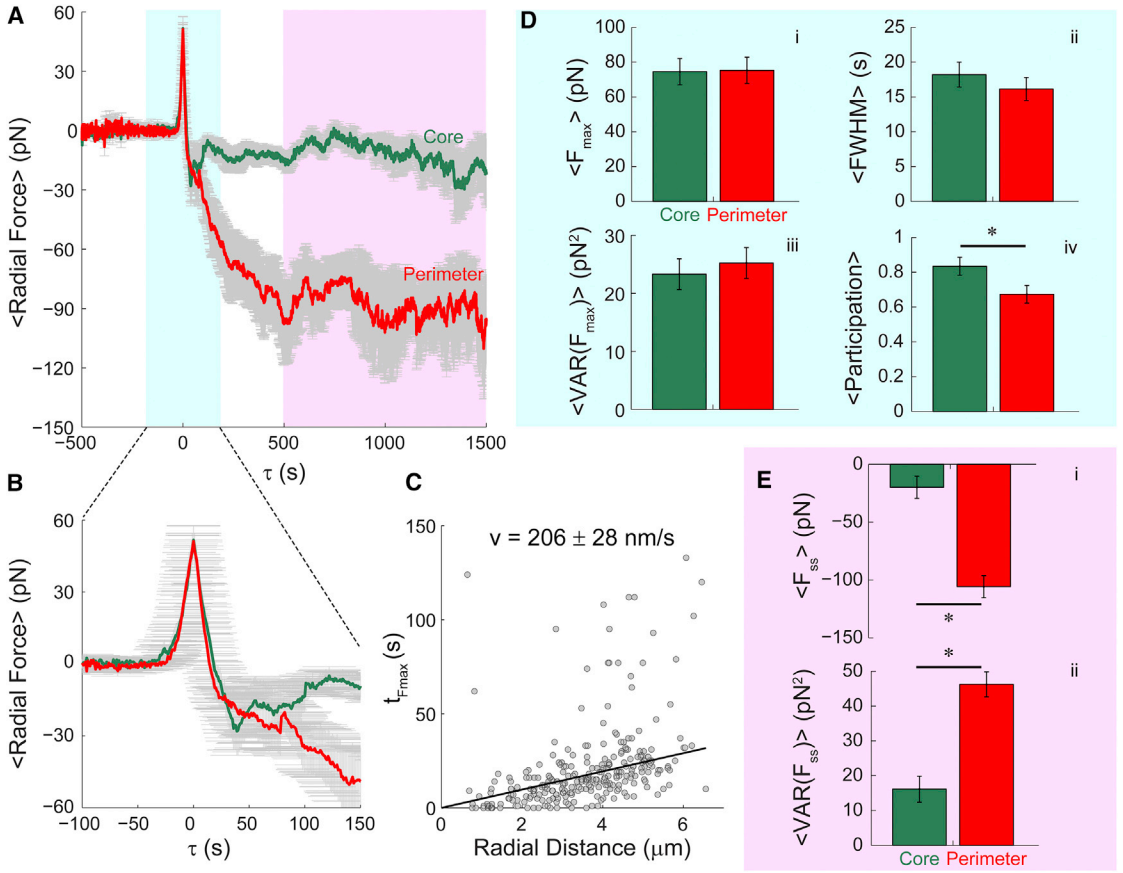

FIGURE 3 Characterizing protrusion and contraction using the ensemble of neutrophil spreading events. (*A*) Mean radial force trajectories of core (*green*) and perimeter (*red*) posts. The transient protrusive and steady-state contractile regimes are denoted by the cyan and lavender shaded regions, respectively. (*B*) An expanded temporal resolution of the protrusive regime in Fig. 3 *A*. (*C*) The time at which protrusive force is maximal as a function of radial distance from the cell centroid. Cell fits are shown in Fig. S3. (*D*) Mean metrics of transient protrusion: (*i*) force maximum, (*ii*) protrusion duration via full width at half force maximum, (*iii*) variance in the ensemble of force maxima, and (*iv*) the fraction of posts in each geometric group that exhibited a protrusive spike (i.e., the participation ratio). (*E*) Mean metrics of steady-state contraction: (*i*) force (*ii*) variance in the ensemble of mean steady-state force. All error bars are ± standard error of the mean ($n = 14$ cells). Asterisk denotes significant difference between populations as computed by post hoc Tukey least significant difference method ($p < 0.05$).

activation shares certain scaffolding proteins (e.g., SLP-76) with outside-in activation in neutrophils, the pathways are not identical (25).

Biochemical perturbations of the cell cytoskeleton

To study the role of the cytoskeleton during neutrophil spreading on post arrays, we pretreated quiescent cells with small molecule inhibitors targeting various cytoskeletal components. Actin in a quiescent neutrophil is confined to a thin cortical shell proximal to the cytoplasmic membrane (26). It has been demonstrated that this actin shell gives rise to cortical tension (19,20). We began by considering the effect of jasplakinolide on neutrophil spreading. Jasplakinolide is a cyclic depsipeptide capable of polymerizing and stabilizing filamentous actin (27). In neutrophils, pretreatment with jasplakinolide has been shown to increase the rigidity of the cortex as measured by micropipette aspiration (20). When we treated quiescent neutrophils with jasplakinolide, the ability of the cells to spread was completely eliminated (Movie S2). Interestingly, the cells were still able to sense the presence of the FN as detected by the formation of small processes uniformly decorating the cell body, as seen with brightfield imaging. These processes were never observed in untreated control cells. It is unclear whether the effect of jasplakinolide in our cells was to stabilize existing F-actin structure or deplete a pool of free actin by polymerizing excess F-actin.

Unlike jasplakinolide, cytochalasin B has been shown to decrease cortical rigidity in neutrophils as measured by micropipette aspiration (19). Cytochalasin B is known to dramatically reduce the rate of actin polymerization and simultaneously interfere with filament-filament interactions that stabilize the actin network (28). When treated with cytochalasin B, our neutrophils were still able to spread but with a substantially reduced velocity of 61 ± 37 nm/s

(see Fig. 4 *B*). During spreading, the mean protrusive force exerted per post was not significantly different than observed with untreated cells. However, the duration of the protrusive event was longer as seen by a significant increase in the full width at half max force (see Fig. 4 *C*, ⟨FWHM⟩). Inhibition of actin polymerization and filament-filament interaction by cytochalasin B had long-term effects as well, significantly decreasing the achieved steady-state contractile force of perimeter posts (Fig. 4 *C*, ⟨Fss⟩) and eliminating the contractile rebound of core posts (Fig. 4 *A*, *Cytochalasin B*). Considered in the context of the results with jasplakinolide, spreading requires relaxation of the actin cortical shell.

We next considered whether spreading was conceptually analogous to lamellipodium formation by inhibiting Arp2/3, the actin-binding protein necessary for filament branching (29). CK666 inhibits Arp2/3-mediated branching by stabilizing the inactive conformation of the seven subunit complex (30). CK666 had no effect on the protrusive capacity of the spreading cells. These cells were not significantly different in the forcefulness or duration of protrusion than their untreated counterparts. That CK666 did not abrogate protrusion suggests the shape change associated with spreading was not analogous to lamellipodium formation, in which Arp2/3 is known to play a critical role (29). However, in response to CK666, we did observe a significant increase in the variance of the forces exerted on core posts during steady-state contractility (Fig. 4 *C*, ⟨VAR(Fss)⟩). This result suggests that a competent actin network might normally dampen post contractility in the core.

Finally, we hypothesized that steady-state contractility would be ROCK and myosin II mediated (17) and tested this by treating neutrophils with Y27632 and blebbistatin (31), respectively. In both cases these inhibitors significantly reduced steady-state contractility (Fig. 4 *C*, ⟨Fss⟩) of perimeter posts but did not eliminate the contractile rebound following protrusion (Fig. 4 *A*, *Y27632* and *Blebbistatin*). In untreated neutrophils, this contractile rebound was only

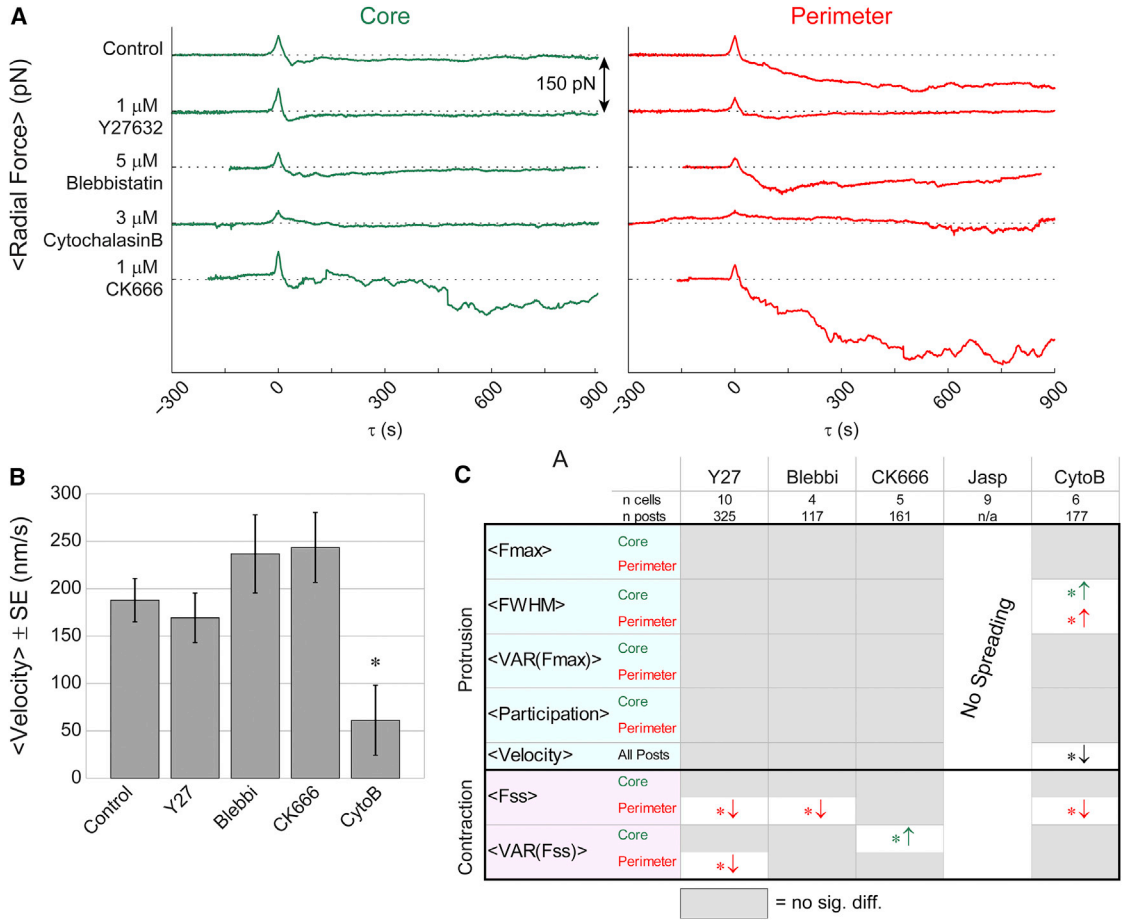

FIGURE 4 Cytoskeletal perturbation via small molecule inhibitors. (*A*) Mean radial force trajectories of the ensemble of individual cell spreading events observed after 30 min pretreatment with the stated inhibitor. Trajectories were plotted at 150 pN intervals. (*B*) Effect of inhibitors on spreading velocity. (*C*) Effect of inhibitors on metrics of protrusion (*cyan shading*) and contraction (*lavender shading*). Asterisk denotes significant difference relative to control computed by post hoc Tukey-Kramer multiple comparisons method ($p < 0.05$). Direction of arrow indicates the direction in which the inhibitor shifted the metric relative to the control, if a significant difference was found.

observed in the core posts. Treating with Y27632 and blebbistatin revealed that the transient rebound was also occurring in the perimeter posts but was obscured when ROCK- and myosin II-mediated contractility commenced. Thus, the transient contractile rebound is a feature of both core and perimeter posts but masked by long-term engagement of the actomyosin-mediated contractile apparatus at the cell periphery. The implication of this result is that the short-term transient rebound is not actomyosin dependent.

Spreading is haptokinetically induced

Neutrophil spreading is induced by haptokinetic interaction with the printed FN. On the soft post arrays (G ~5 kPa) used in our traction measurements, cells assumed a sessile drop morphology (Fig. 5, *A iii*) as captured by spinning disk confocal microscopy z-stacks. The presence of the FN was critical in supporting the transition from a quiescent to spread phenotype. When posts are blocked with Pluronic but not printed with FN (Fig. 5 *A*, *i*), the cells remained spherical and there was no nonspecific adhesion. Additionally, integrin ligation by FN was required upstream of spreading, because pretreating quiescent neutrophils with an antibody against β_2 impeded spreading (Fig. 5 *A*, *ii*). Haptokinetically induced neutrophil spreading via β_2 integrins is consistent with our published observation that a portion of quiescent neutrophils could be induced to migrate on continuous fields of FN without concurrent or prior stimulation by chemoattractant or selectin ligation and that this adhesion was mediated by the integrin MAC-1 ($\alpha_M\beta_2$) (15).

We hypothesized that the vertical profile of neutrophils on post arrays had a stiffness dependence and considered the cell shape when spreading on stiff arrays (G ~42 kPa) and extremely stiff, flat polydimethylsiloxane (PDMS) (G ~833 kPa). On stiff posts the height (i.e., z-extent) of the cell was reduced (Fig. 5 A, *iv*) compared to that observed on flat PDMS printed with continuous fields of FN (Fig. 5 *A*, *v*). Using Fiji (32), we fit ellipses to the vertical profiles and computed the aspect ratio (i.e., ratio of the major axis length to minor axis length). A clear monotonic trend was observed where aspect ratio of the cell increased as stiffness increased (Fig. 5 *B*). The dependency of spread area and aspect ratio on discrete post arrays of increasing stiffness is analogous to that observed of neutrophils on continuous polyacrylamide gels of increasing stiffness (33–35). Thus, as established traction methodologies, PDMS post arrays and polyacrylamide gel systems are complementary tools in probing immune cell mechanobiology.

The FN-null and anti-β_2 controls had similar aspect ratios close to unity (unity denotes a perfect circle). Monotonic trends in circularity, roundedness, and XY cell-substrate contact area as a function of stiffness were observed as well (Fig. S4). These results demonstrate that in our system the FN is required for neutrophils to spread in a β_2 integrin-dependent manner and that the extent of spreading increases as a function of underlying stiffness. We explored a larger range of stiffnesses than Bashour et al., which may explain why XY spread area increases as a function of stiffness in neutrophils but not in T-lymphocytes.

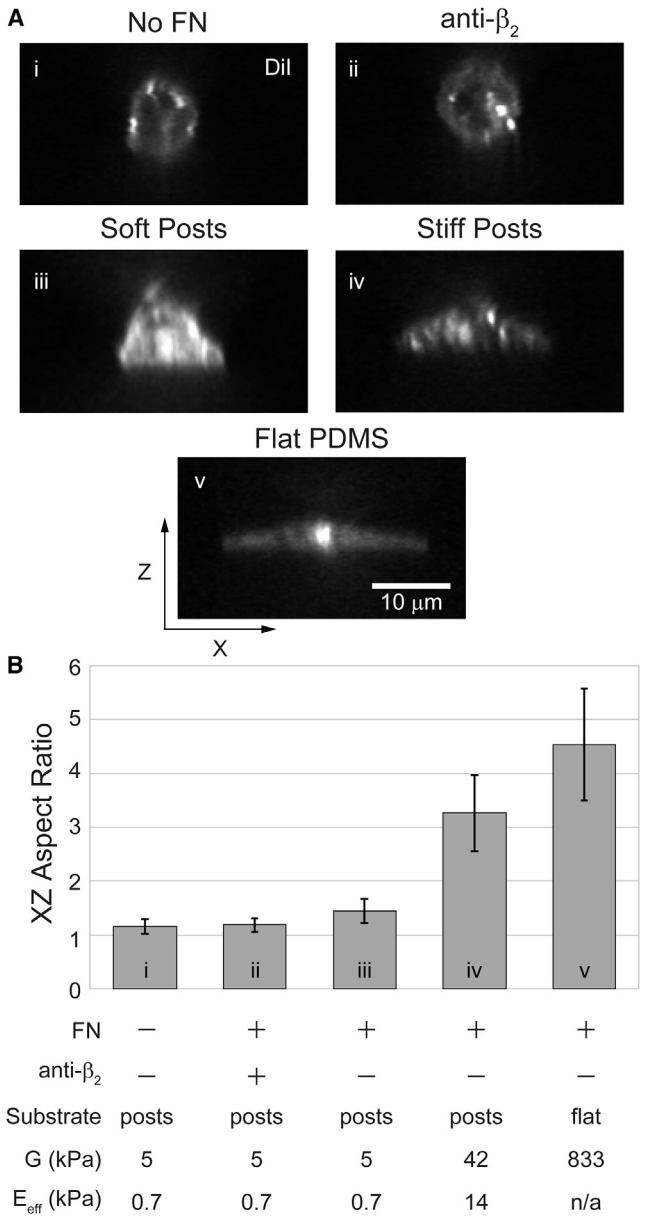

FIGURE 5 Vertical profiles of DiI-labeled neutrophils imaged via confocal microscopy. (*A*) (*i*) An unspread neutrophil on an array of posts blocked with Pluronic F-127, but not printed with FN. (*ii*) An unspread neutrophil on soft FN posts, pretreated with anti-β_2 integrin antibody. (*iii*) A spread neutrophil on soft FN posts used in traction mapping. (*iv*) A spread neutrophil on stiffer FN post arrays. (*v*) A highly spread neutrophil on extremely stiff, flat FN fields. (*B*) Aspect ratio of best-fit ellipses to neutrophil profiles. Error bars are ± standard deviation (n = 8–15 cells per condition). Additional metrics showing similar monotonic trends are reported in Fig. S4. Estimates of shear moduli (G) and effective Young's moduli (E_{eff}) are discussed in the Supporting Material.

Origin of the protrusive signal

Simultaneous acquisition of the cell profile and plane of FN printed post tips revealed that neutrophils moderately invaginate the post arrays to a depth of ~1 μm (see the Supporting Material for estimate of sidewall printing) (Fig. 6 *A*). Our prior experience with neutrophils on continuous fields of FN on PDMS blocked with Pluronic F-127 (15) and the absence of spreading in the present FN-null experiments suggests that invagination was a consequence of printing adhesive ligand on the post sidewalls. Sidewall printing may have resulted from using soft stamps to print the post arrays coupled with the fact that the post tips themselves were rounded.

During spreading, posts beneath the propagating cell front reported the forces associated with the cell's shape change from quiescence (spherical) to spread (sessile drop). This was facilitated by the fact that the cell was not spreading exclusively across the top of the plane of post tips but rather through a volume of finite thickness dictated by the extent of sidewall printing. The posts reported the force of shape change because they physically resided within the cell's spreading path (Fig. 6 *B*, *i*). Our inhibitor studies showed that ROCK- and myosin II-mediated contractility was not fully mature until ~500 s after peak protrusive force was generated. We know that FN was required for spreading as FN-null experiments did not induce shape change. Thus, to claim that protrusion was the result of cell spreading across the plane of post tips but not through a finite volume suggests that integrin ligation of FN was responsible for the ~75 pN/post protrusive force at short times without mature connection to the actomyosin substructure, which requires minutes to develop. If sidewall printing were not present, we would have been unable to quantify the force associated with this transformation as connection of the mature actomyosin substructure to the integrin adhesive contacts at the cell-post interface requires minutes to develop.

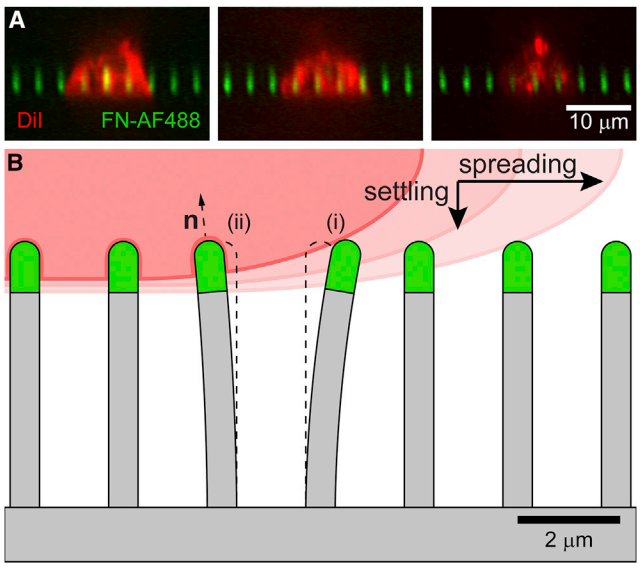

FIGURE 6 Post invagination as origin of protrusion. (*A*) Confocal XZ profiles of DiI-labeled neutrophils on FN-AF488 post arrays. Each field of view is a different neutrophil. (*B*) Schematic of 1) cell spreading through a finite volume of posts as driven by sidewall printing and 2) a conjecture that the transient contractile rebound is driven by local membrane curvature where n is a unit normal vector. Schematic is to scale. Extent of sidewall printing was estimated at 1 μm (calculation in Supporting Material).

The energy of the MAC-1/FN interaction was estimated to be within an order of magnitude of the energy necessary to achieve the spherical-to-sessile drop transformation resisted by the cortical tension of quiescent neutrophils (see Supporting Material for calculation). That adhesion energy alone was not in excess of the required deformation energy to achieve spreading suggests an additional mechanism was at play. Our jasplakinolide and cytochalasin B inhibitor studies point to the release of cortical tension as a possible biophysical mechanism neutrophils employ to permit adhesion-driven spreading and invagination. Additionally, the observation of moderate post invagination suggests a possible explanation as to the origin of the transient contractile rebound present in untreated core posts and ROCK/myosin II-inhibited perimeter posts. We hypothesize that this rebound results from the invaginated posts assuming a transient orientation normal to the cell membrane to minimize the energy of the membrane-post interface (Fig. 6 *B*, *ii*). Future experiments using time-resolved superconfocal microscopy may be able to quantify the post tip orientation relative to the local membrane curvature during spreading. Additionally, future experiments using arrays with a sparse number of nonprinted posts could shed light on the mechanical role of integrin ligation during protrusion.

CONCLUSIONS

As first responders to tissue trauma and infection, neutrophils are capable of fast and dramatic shape changes (3). In this work, we studied the mechanics associated with a neutrophil's transition from a quiescent sphere to a spread and integrin-adherent morphology. In vivo spherical neutrophils circulate throughout the vasculature with their shape maintained by an actin cortical shell. Others have demonstrated, using micropipette aspiration, that this shell possesses a characteristic rigidity, tunable by small molecule inhibitors of actin polymerization (20) and depolymerization (19). By observing neutrophil spreading on post arrays in the presence and absence of such inhibitors, we quantified protrusive forces associated with spreading and attributed their origin to a biophysical mechanism involving a competition of adhesion energy, cortical tension, and the relaxation of that cortical tension.

Neutrophils were induced to spread on FN printed post arrays as a result of their haptokinetic interaction with the

adhesive ligand alone. This was consistent with our previous demonstration that a fraction of neutrophils in contact with continuous fields of FN could spread and migrate without prior or concurrent stimulation by selectin or chemoattractant (15). This haptokinetic spreading was mediated by the $\alpha_M\beta_2$ (MAC-1) integrin, a promiscuous receptor of multiple adhesive ligands. Our work with haptokinetically activated neutrophils suggests MAC-1 promiscuity may serve as a biological safeguard, allowing neutrophils to activate at sites of trauma without executing the earliest rolling stages of the leukocyte adhesion cascade.

On flexible post arrays neutrophil spreading was mechanically detected as a circumferential ring of protrusive force (~75 pN/post) that propagated radially outward (~200 nm/s) until the cell reached its maximum spread area. The magnitude of the protrusive force was invariant with respect to the post's location beneath the cell. Treatment of neutrophils with CK666, an inhibitor of actin branching, had no effect on protrusion suggesting the protrusive phenomenon was not analogous to lamellipodium formation. However, small molecule inhibitors of actin polymerization and depolymerization did reveal that the quiescent-to-spread shape change required relaxation of the quiescent actin cortical shell. Stiffening cortical actin via jasplakinolide treatment completely eliminated spreading, whereas softening cortical actin via cytochalasin B treatment slowed spreading velocity (~60 nm/s). Immediately after maximum protrusion, cell-engaged posts underwent a rapid contractile rebound. At the periphery of the contact zone this contractile rebound continuously evolved into a sustained contractile force floor (~100 pN/post) that was fivefold greater in magnitude than the transient contractile dip experienced in the core (~20 pN/post). Although initial protrusion was myosin II independent long-term sustained contractility was ROCK and myosin II dependent as demonstrated by treatment of neutrophils with Y27632 and blebbistatin, respectively.

Treating cell spreading as a competition between the energy of adhesion driving the cell to spread and the cell's cohesive forces resisting shape change has a long history (36). The equilibrium shape of such a droplet in an aqueous medium is described by Young's equation relating the angle of the droplet-substrate interface to the substrate-medium, droplet-medium, and substrate-droplet interfacial energies. Historically, micropipette aspiration of quiescent neutrophils has motivated their treatment as viscous liquid droplets with apparent surface tension (19,37–40). Recently, Cuvelier and coworkers (41) developed an alternative model of cell spreading, validated in mesenchymal carcinoma cells and biotinylated red blood cells, which treats the cell as a liquid droplet surrounded by a viscous shell of finite thickness. The model predicts two spreading regimes: contact radius evolves as $R \sim t^{0.5}$ at short times and $R \sim t^{0.25}$ at long times when the adhesive patch is comparable to the size of the cell. Although we have limited resolution of the evolution of the spreading neutrophil's contact interface with time, as a result of tracking discretized post tips and not the cell membrane itself, we can approximate the spreading velocity in terms of the propagation rate of the radial protrusive force (Figs. 3 *C* and 4 *B*). We estimate that our neutrophil contact interface grows as $R \sim t^{0.4}$ which is consistent with our previous observations of neutrophil spreading on FN (5) and approaches the short-term $R \sim t^{0.5}$ dependency predicted by the Cuvelier model.

However, there are potentially significant differences. In particular, the contact interface in the Cuvelier model and RICM spreading experiments grows as a radially symmetric disk. In neutrophils this symmetry is absent. In fact, the regions of intimate cell-substrate contact are found to decorate the neutrophil's periphery as a ring with virtually no intimate contact at the core (5). An additional discrepancy is the observation that cytochalasin B softening of the cortical shell decreases spreading velocity in neutrophils; however, Cuvelier and coworkers showed cytochalasin D treatment in HeLA cells increased the spreading velocity. This later observation coupled with the additional finding that spreading is abrogated in the absence of integrin ligation of FN suggests that cell signaling is critical to drive cell spreading and a purely physical treatment of neutrophil spreading is insufficient to reconcile the complete body of experimental work.

Our work extends previous measurements of neutrophil spreading via RICM (5) and reveals that regions of close membrane-substrate contact are also regions of high-force generation. Our studies also complement recent investigation into the mechanics of T-lymphocyte activation on mPADs (12) by considering the role of the cell cytoskeleton and demonstrating that relaxation of cortical tension is a critical driver of cell shape change. Physiologically, the forces associated with this quiescent-to-spread transition have not been considered as a possible pre-extravasation signal that facilitates transendothelial migration. Work by Rabodzey and coworkers (42) on the forces associated with neutrophil extravasation at endothelial cell junctions demonstrated that nN protrusive forces are exerted by neutrophils when rupturing VE-cadherin junctions. These nN forces were attributed directly to neutrophil transmigration and not neutrophil-induced endothelial contraction. That the spherical-to-spread shape change has pN protrusive forces, whereas neutrophil transmigration is a protrusive phenomenon of nN scale suggests a synergistic relationship between transmigrating neutrophils and the underlying endothelial cells.

Future topics to be addressed include the origin of the transient contractile rebound observed in core posts and in the periphery when ROCK/myosin II are inhibited, as well as the organization of the cortical actin shell around posts during invagination. Additionally, work by Ghassemi and coworkers (10) showed that myosin contractile units form linear chains spanning multiple submicron diameter posts as compared to forming closed rings around single micron

diameter posts. In our study of adhesion-driven spreading of neutrophils on submicron diameter posts, we observe motion or chatter in the spatial position of cell engaged posts. We hypothesize that such motion is biochemically correlated with the organization of these linear contractile units. Furthermore, if these mechanical linkages exist in neutrophils, studies could be performed to search for resulting correlations in neighboring posts. These experiments would be most powerful if the actin cytoskeleton were labeled and would be the subject of future work.

The role of β_2 clustering in adhesion-driven neutrophil spreading on post arrays also remains an open question. β_2 clustering and downstream cytoskeletal rearrangement are critical to neutrophil processes such as reactive oxygen intermediate generation and enzyme secretion (43). Yu and coworkers (44) demonstrated that β_3 integrin clustering and radially outward motion of these clusters was upstream of mesenchymal cell spreading on supported lipid bilayers functionalized with RGD and that the basis of the radial motion was actin polymerization. In neutrophils, pretreatment with cytochalasin B, an inhibitor of actin polymerization, slowed but did not eliminate spreading. However, a notable difference from the Yu work is that neutrophils on FN printed post arrays spread an order of magnitude faster than mesenchymal cells on supported lipid bilayers functionalized with RGD (~200 nm/s vs. ~20 nm/s).

SUPPORTING MATERIAL

Supporting Materials and Methods, eight figures, and two movies are available at http://www.biophysj.org/biophysj/supplemental/S0006-3495(15)00660-8.

AUTHOR CONTRIBUTIONS

S.J.H. designed and executed experiments, analyzed data, and wrote the article. C.S.C. provided mPADs masters and helped write the article. J.C.C. consulted on design of analysis routines, data interpretation, and helped write the article. D.A.H. supported the work, consulted on data interpretation, and helped write the article.

ACKNOWLEDGMENTS

We are grateful to Michael T. Yang, PhD for his time and expertise in teaching us mPADs production and printing. Funding for this work was provided by the National Institutes of Health grant HL18208 to D.A.H.

SUPPORTING CITATIONS

References (45–50) appear in the Supporting Material.

REFERENCES

1. McDonald, B., K. Pittman, …, P. Kubes. 2010. Intravascular danger signals guide neutrophils to sites of sterile inflammation. *Science.* 330:362–366.
2. Nathan, C. 2006. Neutrophils and immunity: challenges and opportunities. *Nat. Rev. Immunol.* 6:173–182.
3. Ley, K., C. Laudanna, …, S. Nourshargh. 2007. Getting to the site of inflammation: the leukocyte adhesion cascade updated. *Nat. Rev. Immunol.* 7:678–689.
4. Lomakina, E. B., G. Marsh, and R. E. Waugh. 2014. Cell surface topography is a regulator of molecular interactions during chemokine-induced neutrophil spreading. *Biophys. J.* 107:1302–1312.
5. Sengupta, K., H. Aranda-Espinoza, …, D. Hammer. 2006. Spreading of neutrophils: from activation to migration. *Biophys. J.* 91:4638–4648.
6. Tan, J. L., J. Tien, …, C. S. Chen. 2003. Cells lying on a bed of microneedles: an approach to isolate mechanical force. *Proc. Natl. Acad. Sci. USA.* 100:1484–1489.
7. Lemmon, C. A., N. J. Sniadecki, …, C. S. Chen. 2005. Shear force at the cell-matrix interface: enhanced analysis for microfabricated post array detectors. *Mech. Chem. Biosyst.* 2:1–16.
8. du Roure, O., A. Saez, …, B. Ladoux. 2005. Force mapping in epithelial cell migration. *Proc. Natl. Acad. Sci. USA.* 102:2390–2395.
9. Sniadecki, N. J., C. M. Lamb, …, D. H. Reich. 2008. Magnetic microposts for mechanical stimulation of biological cells: fabrication, characterization, and analysis. *Rev. Sci. Instrum.* 79:044302.
10. Ghassemi, S., G. Meacci, …, J. Hone. 2012. Cells test substrate rigidity by local contractions on submicrometer pillars. *Proc. Natl. Acad. Sci. USA.* 109:5328–5333.
11. Ricart, B. G., M. T. Yang, …, D. A. Hammer. 2011. Measuring traction forces of motile dendritic cells on micropost arrays. *Biophys. J.* 101:2620–2628.
12. Bashour, K. T., A. Gondarenko, …, L. C. Kam. 2014. CD28 and CD3 have complementary roles in T-cell traction forces. *Proc. Natl. Acad. Sci. USA.* 111:2241–2246.
13. Yang, M. T., J. Fu, …, C. S. Chen. 2011. Assaying stem cell mechanobiology on microfabricated elastomeric substrates with geometrically modulated rigidity. *Nat. Protoc.* 6:187–213.
14. Schoen, I., W. Hu, …, V. Vogel. 2010. Probing cellular traction forces by micropillar arrays: contribution of substrate warping to pillar deflection. *Nano Lett.* 10:1823–1830.
15. Henry, S. J., J. C. Crocker, and D. A. Hammer. 2014. Ligand density elicits a phenotypic switch in human neutrophils. *Integr Biol (Camb).* 6:348–356.
16. Penberthy, T. W., Y. Jiang, …, D. T. Graves. 1995. MCP-1-stimulated monocytes preferentially utilize beta 2-integrins to migrate on laminin and fibronectin. *Am. J. Physiol.* 269:C60–C68.
17. Stroka, K. M., H. N. Hayenga, and H. Aranda-Espinoza. 2013. Human neutrophil cytoskeletal dynamics and contractility actively contribute to trans-endothelial migration. *PLoS One.* 8:e61377.
18. Hui, K. L., L. Balagopalan, …, A. Upadhyaya. 2015. Cytoskeletal forces during signaling activation in Jurkat T-cells. *Mol. Biol. Cell.* 26:685–695.
19. Tsai, M. A., R. S. Frank, and R. E. Waugh. 1994. Passive mechanical behavior of human neutrophils: effect of cytochalasin B. *Biophys. J.* 66:2166–2172.
20. Sheikh, S., W. B. Gratzer, …, G. B. Nash. 1997. Actin polymerisation regulates integrin-mediated adhesion as well as rigidity of neutrophils. *Biochem. Biophys. Res. Commun.* 238:910–915.
21. Jannat, R. A., M. Dembo, and D. A. Hammer. 2011. Traction forces of neutrophils migrating on compliant substrates. *Biophys. J.* 101:575–584.
22. Kilfoil, M. L. 2014. Biological Physics Kilfoil Lab. Web Page. 04 November 2014. http://people.umass.edu/kilfoil/downloads.html.
23. Pelletier, V., N. Gal, …, M. L. Kilfoil. 2009. Microrheology of microtubule solutions and actin-microtubule composite networks. *Phys. Rev. Lett.* 102:188303.
24. Crocker, J. C., and D. G. Grier. 1996. Methods of digital video microscopy for colloidal studies. *J. Colloid Interface Sci.* 179:298–310.

25. Jordan, M. S., and G. A. Koretzky. 2010. Coordination of receptor signaling in multiple hematopoietic cell lineages by the adaptor protein SLP-76. *Cold Spring Harb. Perspect. Biol.* 2:a002501.

26. Sheterline, P., and C. R. Hopkins. 1981. Transmembrane linkage between surface glycoproteins and components of the cytoplasm in neutrophil leukocytes. *J. Cell Biol.* 90:743–754.

27. Holzinger, A. 2009. Jasplakinolide: an actin-specific reagent that promotes actin polymerization. *Methods Mol. Biol.* 586:71–87.

28. MacLean-Fletcher, S., and T. D. Pollard. 1980. Mechanism of action of cytochalasin B on actin. *Cell.* 20:329–341.

29. Svitkina, T. M., and G. G. Borisy. 1999. Arp2/3 complex and actin depolymerizing factor/cofilin in dendritic organization and treadmilling of actin filament array in lamellipodia. *J. Cell Biol.* 145:1009–1026.

30. Hetrick, B., M. S. Han, …, B. J. Nolen. 2013. Small molecules CK-666 and CK-869 inhibit actin-related protein 2/3 complex by blocking an activating conformational change. *Chem. Biol.* 20:701–712.

31. Limouze, J., A. F. Straight, …, J. R. Sellers. 2004. Specificity of blebbistatin, an inhibitor of myosin II. *J. Muscle Res. Cell Motil.* 25:337–341.

32. Schindelin, J., I. Arganda-Carreras, …, A. Cardona. 2012. Fiji: an open-source platform for biological-image analysis. *Nat. Methods.* 9:676–682.

33. Jannat, R. A., G. P. Robbins, …, D. A. Hammer. 2010. Neutrophil adhesion and chemotaxis depend on substrate mechanics. *J. Phys.Condens. Matter.* 22:194117.

34. Oakes, P. W., D. C. Patel, …, J. X. Tang. 2009. Neutrophil morphology and migration are affected by substrate elasticity. *Blood.* 114:1387–1395.

35. Stroka, K. M., and H. Aranda-Espinoza. 2009. Neutrophils display biphasic relationship between migration and substrate stiffness. *Cell Motil. Cytoskeleton.* 66:328–341.

36. Carter, S. B. 1967. Haptotaxis and the mechanism of cell motility. *Nature.* 213:256–260.

37. Evans, E., and B. Kukan. 1984. Passive material behavior of granulocytes based on large deformation and recovery after deformation tests. *Blood.* 64:1028–1035.

38. Evans, E., and A. Yeung. 1989. Apparent viscosity and cortical tension of blood granulocytes determined by micropipette aspiration. *Biophys. J.* 56:151–160.

39. Needham, D., and R. M. Hochmuth. 1992. A sensitive measure of surface stress in the resting neutrophil. *Biophys. J.* 61:1664–1670.

40. Lomakina, E. B., C. M. Spillmann, …, R. E. Waugh. 2004. Rheological analysis and measurement of neutrophil indentation. *Biophys. J.* 87:4246–4258.

41. Cuvelier, D., M. Théry, …, L. Mahadevan. 2007. The universal dynamics of cell spreading. *Curr. Biol.* 17:694–699.

42. Rabodzey, A., P. Alcaide, …, B. Ladoux. 2008. Mechanical forces induced by the transendothelial migration of human neutrophils. *Biophys. J.* 95:1428–1438.

43. Raptis, S. Z., S. D. Shapiro, …, C. T. Pham. 2005. Serine protease cathepsin G regulates adhesion-dependent neutrophil effector functions by modulating integrin clustering. *Immunity.* 22:679–691.

44. Yu, C. H., J. B. Law, …, M. P. Sheetz. 2011. Early integrin binding to Arg-Gly-Asp peptide activates actin polymerization and contractile movement that stimulates outward translocation. *Proc. Natl. Acad. Sci. USA.* 108:20585–20590.

45. Desai, R. A., M. K. Khan, …, C. S. Chen. 2011. Subcellular spatial segregation of integrin subtypes by patterned multicomponent surfaces. *Integr Biol (Camb).* 3:560–567.

46. Beer, F. P., E. R. Johnston, and J. T. DeWolf. 2006. Mechanics of Materials. McGraw-Hill Higher Education, Boston, MA.

47. Ghibaudo, M., A. Saez, …, B. Ladoux. 2008. Traction forces and rigidity sensing regulate cell functions. *Soft Matter.* 4:1836–1843.

48. Hecht, E. 1998. Optics. Addison-Wesley, Reading, MA.

49. Diamond, M. S., and T. A. Springer. 1993. A subpopulation of Mac-1 (CD11b/CD18) molecules mediates neutrophil adhesion to ICAM-1 and fibrinogen. *J. Cell Biol.* 120:545–556.

50. Krasik, E. F., K. E. Caputo, and D. A. Hammer. 2008. Adhesive dynamics simulation of neutrophil arrest with stochastic activation. *Biophys. J.* 95:1716–1728.

Biophysical Journal

Supporting Material

Protrusive and Contractile Forces of Spreading Human Neutrophils

Steven J. Henry,[1] Christopher S. Chen,[2] John C. Crocker,[3,*] and Daniel A. Hammer[1,3,*]

[1]Bioengineering, University of Pennsylvania, Philadelphia, Pennsylvania; [2]Biomedical Engineering, Boston University, Boston, Massachusetts; and [3]Chemical and Biomolecular Engineering, University of Pennsylvania, Philadelphia, Pennsylvania

Supporting Material

Henry et al. Protrusive and Contractile Forces of Spreading Human Neutrophils

Media and Reagents (Continued)

Rinsing buffer was Hanks' Balanced Salt Solution (Life Technologies, Carlsbad, CA) without calcium or magnesium supplemented with 10 mM HEPES (Life Technologies) and pH adjusted to 7.4. Storage buffer was rinsing buffer supplemented with 2 mg/mL glucose. Running buffer was storage buffer supplemented with 1.5 mM Ca^{2+} and 2 mM Mg^{2+}. Fibronectin (FN) was from human plasma (BD Biosciences, Bedford, MA). Labeling of FN via Alexa Fluor carboxylic acid, succinimidyl ester (Life Technologies) was performed in accordance with the manufacturer's recommended protocol. The nonionic triblock copolymer Pluronic F-127 (Sigma) was prepared at 0.2% w/v in PBS without calcium and magnesium ("PBS(-)"). Stock delta9-DiI lipophilic membrane dye (Life Technologies) was prepared in 200 proof ethanol at 50 ng/mL. All solutions were sterile filtered or prepared sterile. The bicinchoninic acid protein assay (Pierce Biotechnology, Rockford, Il) was performed on stock FN solutions to measure concentration. Poly(dimethylsiloxane) (PDMS) was Sylgard 184 Silicone Elastomer from Dow Corning (Midland, MI) prepared per the specified weight ratio of base:cure agents, mixed vigorously, and degassed until optically clear. Silane was Trichloro(1H, 1H, 2H, 2H-perfluorooctyl)silane from Sigma (Saint Louis, MO).

Microfabricated-Post-Array-Detectors (mPADs) and Microcontact Printing (Continued)

The positive silicon masters were manufactured in and provided directly by the Chen laboratory. From these positive masters, negative PDMS reliefs were cast then silanized by vapor deposition. Silanized molds were coated with a small amount of 10:1 base:cure (w/w) PDMS and degassed. The 10:1 PDMS for positive casting was carefully weighed using a calibrated analytical balance and thoroughly mixed and degassed before coating the molds. PDMS coated molds were pressed against the oxygen plasma cleaned glass coverslips and leveled in a 110 °C for 20 hr. After curing, molds were released in a shallow dish of 200 proof ethanol and sonicated for 2 min. Posts were recovered in a Samdri-PVT-3D critical point drier (Tousimis, Rockville, MD) and stored in a dessicator jar until use.

25:1 base:cure (w/w) PDMS stamps were cast against a silicon wafer to produce an extremely smooth surface. Stamps were trimmed to approximately 25 mm^2, sonicated in 200 proof ethanol for 10 min, rinsed twice in diH_2O and dried in a gentle stream of filtered $N_{2(g)}$. The surface of the PDMS stamp, previously cast against the silicon wafer, was incubated with 50 μL of 100 μg/mL FN-AF488 in PBS(-) for 1 hr at room temperature (RT). After incubation stamps were rinsed twice in a submerging quantity (~ 50 mL) of diH_2O and dried in a gentle stream of filtered $N_{2(g)}$. Cast mPADs on coverslips were loaded in autoclaved Attofluor chambers (Life Technologies) and rendered hydrophilic by 7 min treatment in ultraviolet ozone (UVO Cleaner Model 342, Jelight, Irvine, CA) (1). Inked stamps were inverted and set atop the UVO treated post tips. After contact the chamber was flooded with 200 proof ethanol and the stamp removed in one quick motion. Posts were observed under fluorescence microscopy to verify printing fidelity and post viability. Subsequently, posts were stained with DiI to facilitate long-duration tracking by incubation for 15 min at RT in the dark. After staining, ethanol was exchanged for PBS(-) via repeated and gentle rinsing. Substrates were blocked against non-specific binding by submerging in 0.2% w/v F127 in PBS(-) and incubating 30 min at RT. After blocking, F127 was

exchanged for PBS(-) by repeated and gentle rinsing with running buffer. Chambers were pre-warmed to 37 °C in a cabinet incubator before cell plating and imaging.

Neutrophil Isolation (Continued)

Whole blood was obtained from human donors via venipuncture and collected in sodium heparin Vacutainers (BD Biosciences). Volunteers were required to be in good health and abstain from alcohol and all over-the-counter medication for 24 hrs prior to donation. Blood samples were allowed to cool to RT for 15 min and layered in a 1:1 ratio of whole blood to Polymorphprep (Axis-Shield, Oslo, Norway). Vials were spun for 45-60 min at 550-650 x *g* and 21 ºC. After separation, the polymorphonuclear band and underlying separation media layer were aspirated into fresh round-bottom tubes. The isolated solution of cells and separation-media was diluted with rinsing buffer and spun for 10 min at 250 x *g* and 21 ºC. Red Blood Cells (RBC) were eliminated from the resulting cell pellet via hypotonic lysis. After lysis, vials were centrifuged for 10 min at 250 x *g* and 21 ºC and the RBC-free pellets resuspended in storage buffer. Neutrophils were stored at 10^6 cells/mL on a tube rotisserie at 4 ºC until time of plating.

Calculation of Post Spring Constant

For a cantilever beam of uniform cross section carrying a load at its unconstrained terminus, the equation of the beam's elastic deformation curve is given by (Eq. 1):

$$F = \left(\frac{3EI}{L^3}\right)\delta \qquad \text{(Eq. 1)}$$

where F, E, I, L and δ are the force exerted at the unconstrained terminus, Young's modulus of the beam material, moment of inertia of the beam cross section, and the resulting deflection respectively (2). The assumption being made is that the beam is subjected to small deflections which do not cause plastic deformation. The terms within the parenthesis of Eq. 1 are collectively referred to as the post spring constant (k_{spring}, Eq. 2):

$$k_{spring} = \frac{3EI}{L^3} \qquad \text{(Eq. 2)}$$

Since our fabrication protocol is identical to Yang et al. (3) we employ their measured Young's modulus for PDMS cured 20 hr at 110 °C of E = 2.5 ± 0.5 MPa. The moment of inertia I for a circular cross section is (Eq. 3):

$$I = \frac{\pi d^4}{64} \qquad \text{(Eq. 3)}$$

Where d is the diameter of the post. Substituting (Eq. 3) into (Eq. 2) yields (Eq. 4):

Supporting Material

Henry et al. Protrusive and Contractile Forces of Spreading Human Neutrophils

$$k_{spring} = \frac{3E\pi d^4}{64L^3} \qquad \text{(Eq. 4)}$$

Using scanning electron microscopy we captured a series of micrographs and measured the post diameter, d = 604 ± 31 nm (m ± sd), and length, L = 5.576 ± 0.286 μm (m ± sd). Using error propagation (Eq. 5) we computed the mean and standard deviation ($\sigma_{k_{spring}}$, Eq. 5) of our empirical spring constant as $k_{spring} = 0.28 \pm 0.09$ pN/nm (m ± sd).

$$\sigma_{k_{spring}} = \sqrt{\left(\frac{\partial k_{spring}}{\partial E}\right)^2 \sigma_E^2 + \left(\frac{\partial k_{spring}}{\partial d}\right)^2 \sigma_d^2 + \left(\frac{\partial k_{spring}}{\partial L}\right)^2 \sigma_L^2} \qquad \text{(Eq. 5)}$$

Work by Schoen et al. (4) demonstrated that in low aspect ratio posts (i.e. posts short compared to their width) substrate warping at the base was a substantial contribution to the observed deflection. The authors constructed a table of correction factors to reduce the apparent spring constant as a function of post aspect ratio. For our posts with L/d = 9.2 the interpolated Schoen et al. reducing factor (assuming Poisson ratio of 0.5) is 7.8%. This correction is less than the propagated error in our empirical spring constant calculation and so we anticipate substrate warping is not a major contribution to the observed deflections in this study.

In the manuscript we quote approximate shear moduli (Fig. 5 *B* "G") computed under the assumption that the mode of cell deformation of the post is shear and exerted over its cross sectional area. This assumption is motivated by the empirical work of Lemmon et al. (5) which demonstrated that shear is a larger contribution to post deflection than torque. Alternatively, Ghibaudo and coworkers developed a theoretical description of effective array stiffness by solution of the Green's function for a discretized substrate (6). The Ghibaudo model estimates the Young's moduli of post arrays as being substantially softer than anticipated by a local pure shear model (Fig. 5 *B* "E_{eff}").

Identification of Cell-Engaged Posts

After trajectory dedrifting, constructing a scatter plot of the variances in the tangential and radial directions reveals two populations of trajectories. A compact cloud of data with low variance corresponds to the posts in the field of view outside of the cell-substrate contact zone. The remaining posts correspond to those within the cell-substrate contact zone and are considered "cell-engaged".

Supporting Material

Henry et al. Protrusive and Contractile Forces of Spreading Human Neutrophils

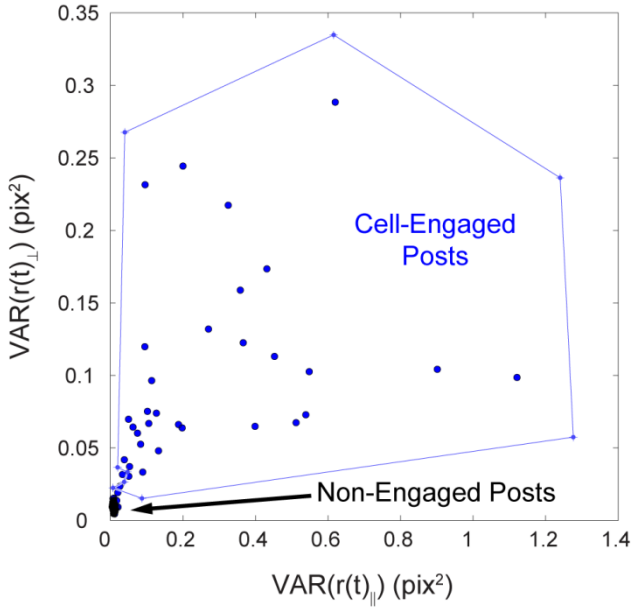

Figure S1. Scatter plot of post trajectory variances in the tangential (⊥) and radial (||) directions for data corresponding to Fig. 1 and 2 of the main text. The compact cloud of posts with low variance corresponds to posts outside the cell-substrate contact zone. The remaining diffuse cloud is declared "cell-engaged" and used in data analysis. 1 pixel = 0.192 μm.

Translation of Post Trajectories

The strong directional bias of peripheral posts (Fig. 1 *D*) towards the cell centroid motivated us to translate post trajectories from a laboratory reference frame (x(t), y(t)) into a cell reference frame ($r_{||}(t)$, $r_{\perp}(t)$). For each post a vector connecting the geometric centroid and the resting lattice position of that post was constructed. This vector was used to position the orthogonal ($r_{||}(t)$, $r_{\perp}(t)$) pair such that the radial axis was parallel with the connecting vector.

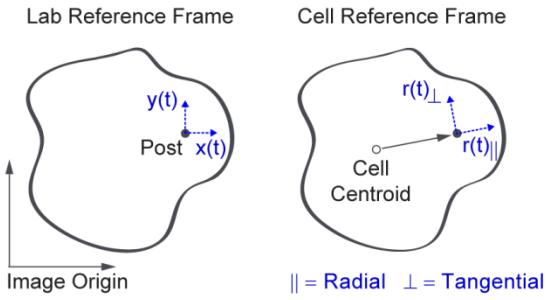

Figure S2. In the lab reference frame post trajectories are positioned relative to the field-of-view origin. A cell reference frame is more intuitive and constructed by translating post trajectories in terms of the orthogonal axes ($r_{||}(t)$, $r_{\perp}(t)$) such that the radial axis is parallel to a vector connecting the geometric centroid of the cell and the resting lattice position of the post.

Supporting Material

Henry et al. Protrusive and Contractile Forces of Spreading Human Neutrophils

Computing a Spreading Velocity

For each cell we constructed a scatter plot of the time at which a post's maximum protrusive force was observed (relative to the first protrusive event which denoted the onset of spreading) as a function of the radial distance of the post from the cell centroid. A best fit linear equation was computed, subject to the constraint $t_{Fmax}(r) = 0$. The inverse of the slope of the curve was the propagation velocity. The mean velocity quoted in the manuscript (Fig. 3 *C*) is the mean and standard error of the ensemble of 14 spreading velocities acquired in this manner.

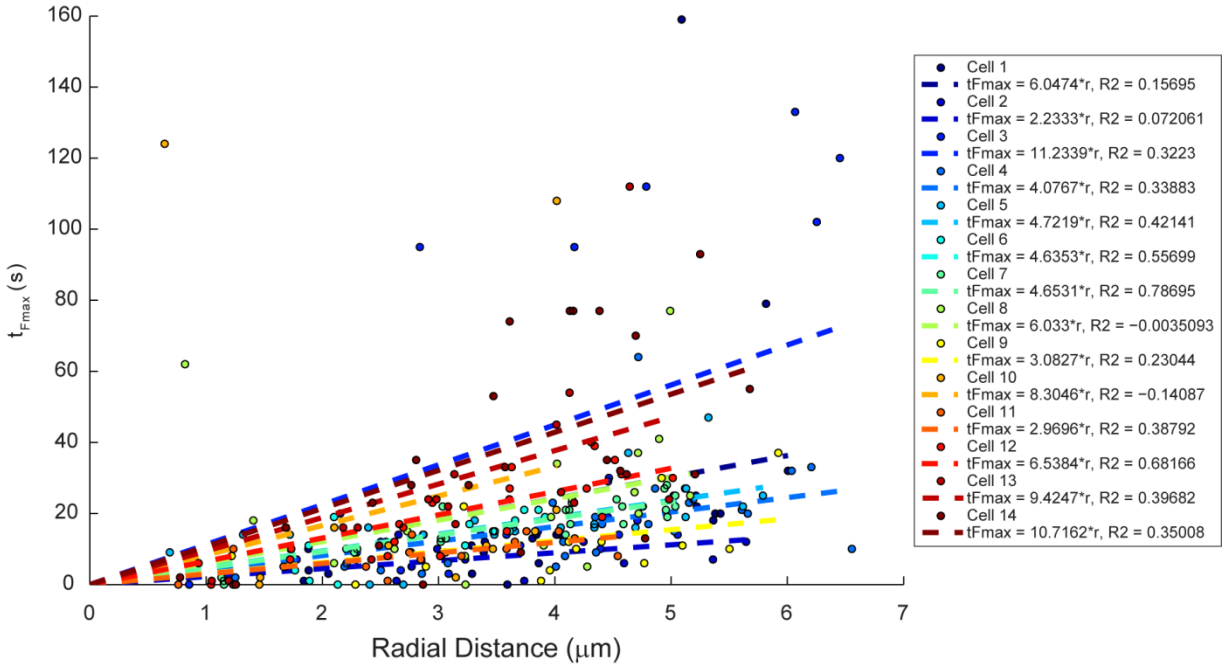

Figure S3. Scatter plots for 14 spreading cells of the time at which a post's maximum protrusive force occurred as a function of the post's radial distance from the cell centroid.

Metrics of Cell Shape

In addition to XZ profile aspect ratio in Fig. 5 *B* of the main text, we used Fiji (7) to compute XZ circularity ($4*\pi*$area/perimeter^2, Fig. S4 *A*), roundedness (1/aspect ratio, Fig. S4 *B*), and XY contact area of the cell-substrate interface (Fig. S4 *C*). As substrate stiffness increases circularity and roundedness monotonically decreased indicating an increasing deviation from a perfect circle. Conversely as substrate stiffness increases the XY contact area monotonically increases. In all metrics FN-null and anti-β_2 conditions were indistinguishable.

Supporting Material

Henry et al. Protrusive and Contractile Forces of Spreading Human Neutrophils

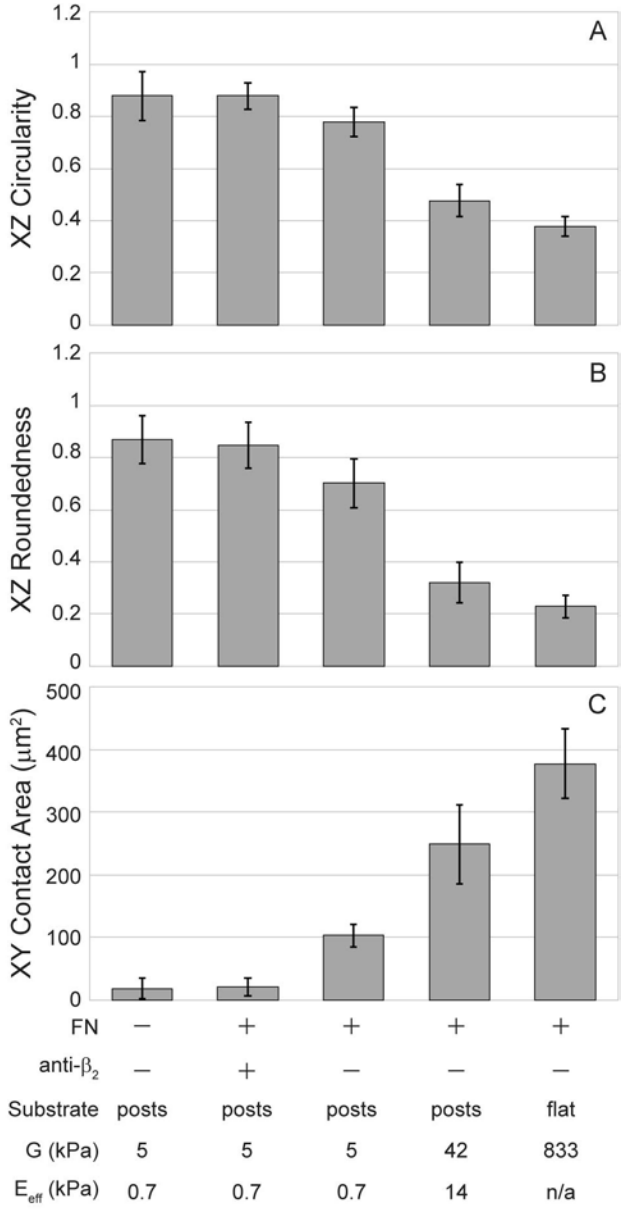

Figure S4. Metrics of XZ and XY cell profile: (A) XZ circularity, (B) XZ roundedness, and (C) XY contact area. Error bars are ± standard deviation (n = 8-15 cells per condition).

Estimating Extent of Post Sidewall Printing

From our confocal z stacks we observe that neutrophils invaginate FN-printed post arrays to the limit of the post sidewall printing (Fig. 6 *A*). The following series of calculations were used to estimate the extent of this sidewall printing and thus depth of invagination. An apparent image (I) is the convolution of the object's intensity profile (F) with the optical system's airy disc (G) (Eq. 6) (8).

Supporting Material

Henry et al. Protrusive and Contractile Forces of Spreading Human Neutrophils

$$I = F \otimes G \qquad \text{(Eq. 6)}$$

Assuming the object's intensity profile and the optical airy disc are reasonably approximated as Gaussian distributions, the convolution of two Gaussians produces a variance (σ^2) that is the sum of the variances (Eq. 7).

$$\sigma_I^2 = \sigma_F^2 + \sigma_G^2 \qquad \text{(Eq. 7)}$$

Using green fluorescent beads (Molecular Probe FluoSpheres, Catalog: F8813, Lot: 1600255) of known size (diameter = 0.49 ± 0.015 μm) we acquired XZ intensity profiles on the spinning disc confocal in the same channel and at the same magnification as our post measurements (Fig. S5 *C*). We normalized each bead intensity profile so the area under the intensity curve equaled unity and the peak of the intensity curve was translated to reside at x = 0 (Fig. S5 *D*).

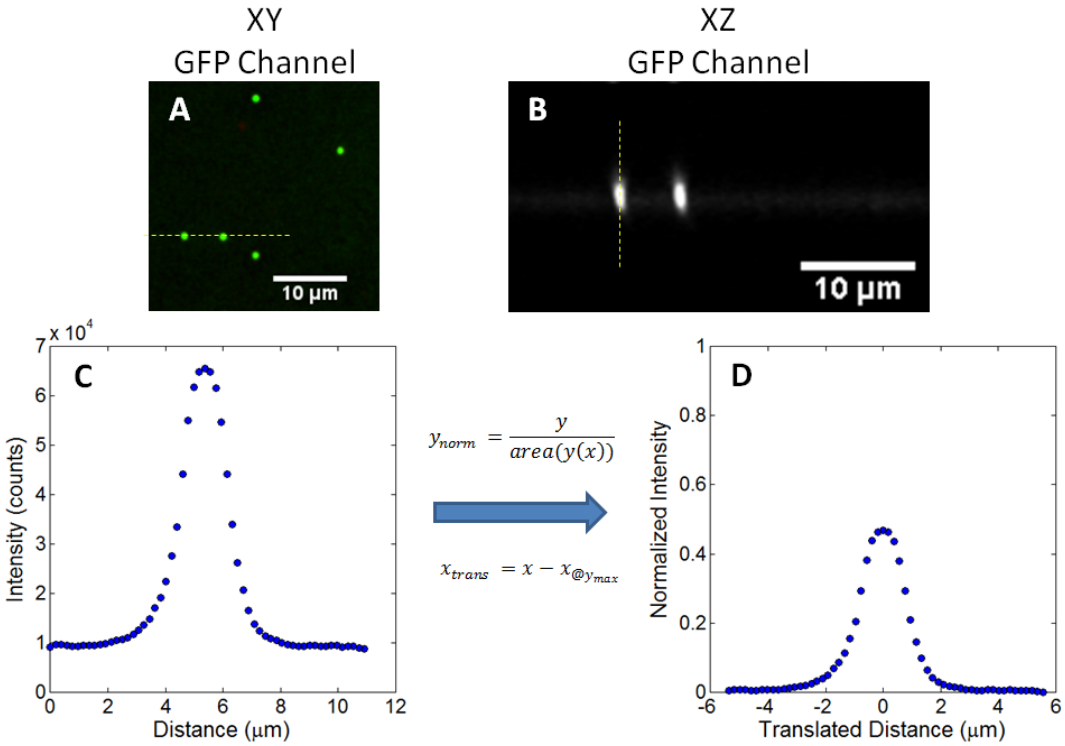

Figure S5. Confocal images of 0.49 μm diameter green fluorescent beads using the same magnification and acquisition settings as post arrays. (A) XY plan view of green fluorescent beads. (B) XZ profile view of green fluorescent beads denoted by yellow dotted line in Fig. S5 *A*. (C) Raw bead intensity along yellow dotted line in Fig. S5 *B*. (D) Normalized bead intensity so area beneath intensity curve equals unity and peak intensity occurs at x = 0.

Next, each normalized bead intensity curve was fit with a two-parameter Gaussian distribution where mean (μ) and standard deviation (σ) were free parameters (Fig. S6). The mean standard deviation of ten beads was 0.94 ± 0.09 μm (m ± sd).

Supporting Material

Henry et al. Protrusive and Contractile Forces of Spreading Human Neutrophils

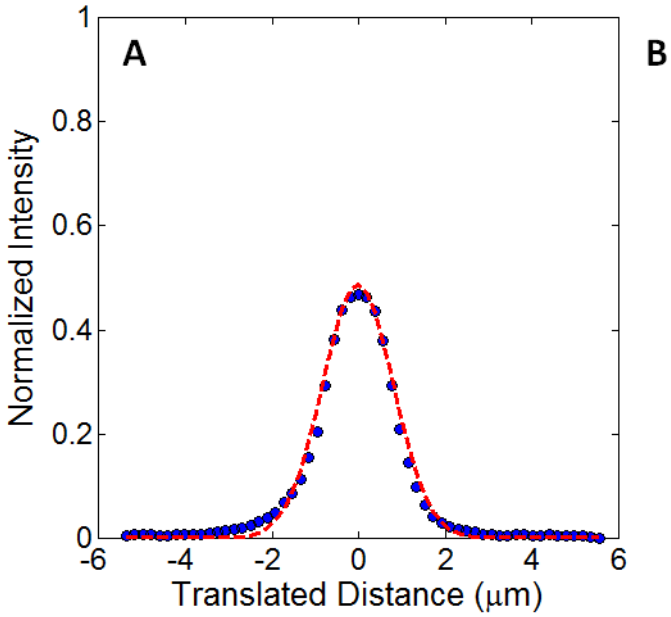

$$y_{fit} = \frac{1}{\sqrt{2\pi\sigma^2}} * e^{\frac{-(x-\mu)^2}{2\sigma^2}}$$

μ = -0.0134 μm

σ = 0.8174 μm

adjusted R2 = 0.99

Average of 10 beads:

$<\sigma_{Image}>$ = 0.94 ± 0.09 μm

Figure S6. Fitting calibration bead intensity plots with a two parameter Gaussian. (A) Intensity plot of Fig. S5 *D* overlaid with its best fit Gaussian curve. (B) Fit parameters corresponding to red-dotted line in Fig. S6 *A*.

To estimate the variance of the Gaussian-approximated optical airy disc we must make an assumption about the unconvolved intensity profile of the fluorescent bead. Let the unconvolved intensity profile of the fluorescent bead have a full width at half maximum (FWHM) equal to the known bead diameter. For a Guassian distribution, FWHM is related to the standard deviation (σ) (Eq. 8) via:

$$FWHM_{bead} = 2\sqrt{2\ln(2)}\sigma_{bead} \qquad \text{(Eq. 8)}$$

Rearranging for σ_{bead} and substituting $FWHM_{bead}$ = 0.49 μm results in (Eq. 9):

$$\sigma_{bead} = \frac{0.49}{2\sqrt{2\ln(2)}} \sim 0.21\mu m \qquad \text{(Eq. 9)}$$

Solving Eq. 7 for the Gaussian-approximation to the confocal's optical airy disc yields (Eq. 10):

$$\begin{aligned} \sigma^2_{optics} &= \sigma^2_{image} - \sigma^2_{bead} \\ \sigma^2_{optics} &= (0.94\mu m)^2 - (0.21\mu m)^2 \\ \sigma^2_{optics} &\sim 0.8403\mu m^2 \end{aligned} \qquad \text{(Eq. 10)}$$

Having approximated the contribution of the optical airy disc to the blurr in the XZ intensity profile of fluorescent beads of known size, we can now quantify the apparent intensity

profile of the printed post arrays and calculate an estimate of the actual extent of sidewall printing. A set of post arrays, printed with FN-AF488 in a manner identical to those used in cell spreading experiments, was imaged in an aqueous solution of 90% glycerol. Glycerol was employed to bring the aqueous refractive index closer to that of cured PDMS (Fig. S7 *A*).

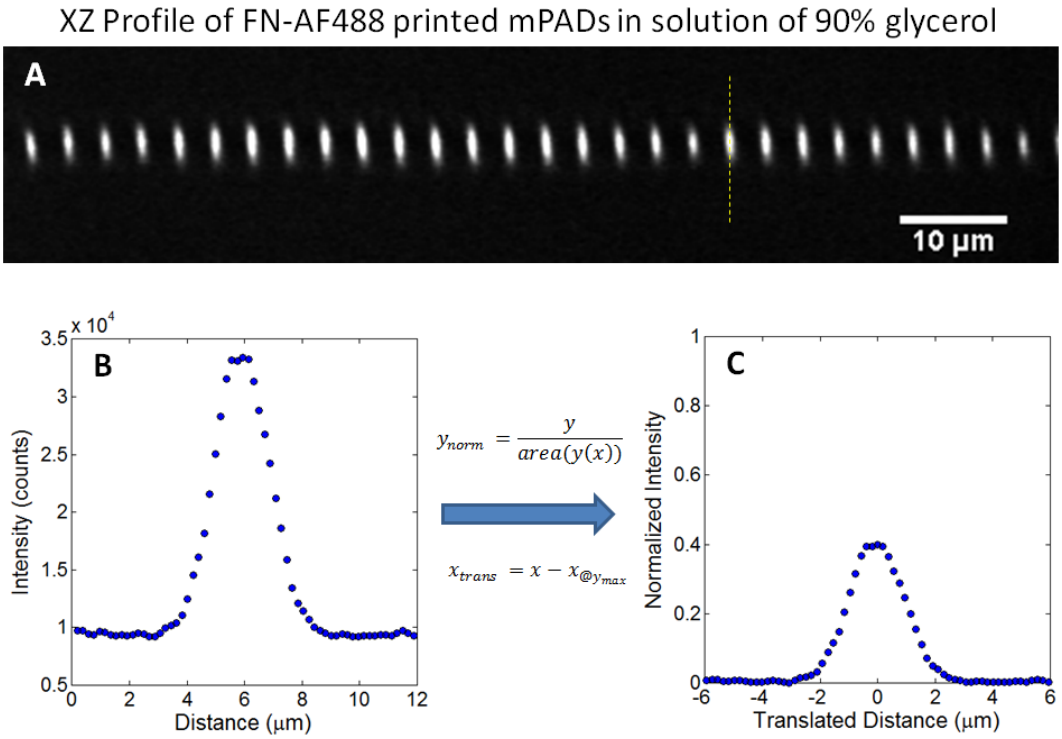

Figure S7. Confocal measurements of FN-AF488 printed post arrays in a solution of 90% glycerol. (A) XZ profile view of printed posts. (B) Raw post intensity along yellow dotted line in Fig. S7 *A*. (C) Normalized post intensity so area beneath intensity curve equals unity and peak intensity occurs at x = 0.

Next, each normalized post intensity curve was fit with a two-parameter Gaussian distribution where mean (μ) and standard deviation (σ) were free parameters (Fig. S8). The mean standard deviation of ten printed posts was 1.00 ± 0.10 μm (m ± sd).

Supporting Material

Henry et al. Protrusive and Contractile Forces of Spreading Human Neutrophils

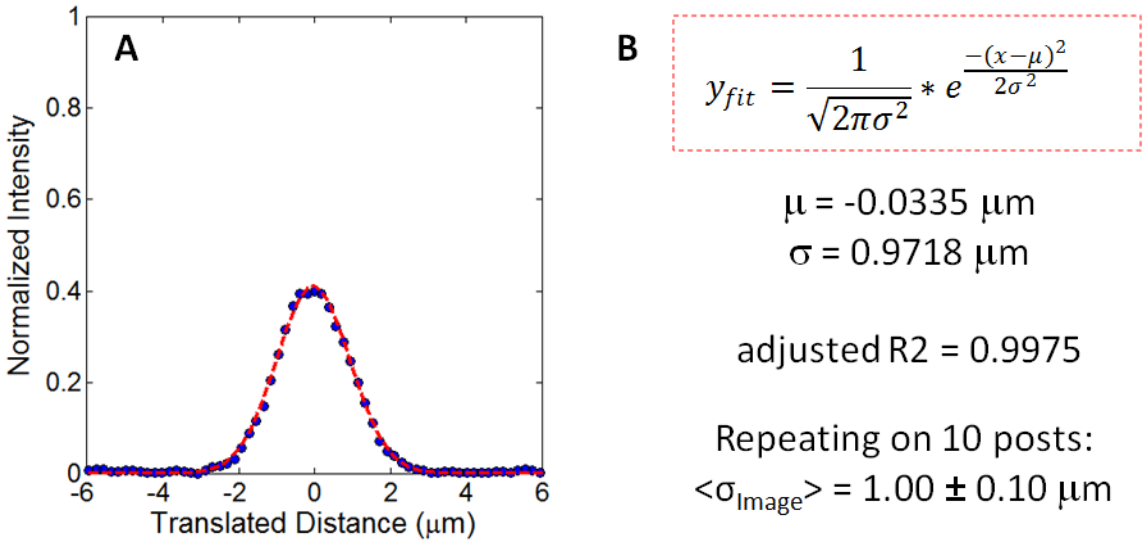

Figure S8. Fitting printed post intensity plots with a two parameter Gaussian. (A) Intensity plot of Fig. S7 *C* overlaid with its best fit Gaussian curve. (B) Fit parameters corresponding to red-dotted line in Fig. S8 *A*.

Solving Eq. 7 for the variance of the Gaussian-approximation to the true intensity profile of printed posts yields (Eq. 11):

$$\sigma_{post}^2 = \sigma_{image}^2 - \sigma_{optics}^2$$
$$\sigma_{post}^2 = (1.00\mu m)^2 - 0.8403\mu m^2 \qquad \text{(Eq. 11)}$$
$$\sigma_{post}^2 \sim 0.1597\mu m^2$$

Lastly, we define the extent of sidewall printing as the FWHM of the unconvolved z-intensity profile (Eq. 12):

$$FWHM_{post} = 2\sqrt{2\ln(2)}\sigma_{post}$$
$$FWHM_{post} = 2\sqrt{2\ln(2) * 0.1597\mu m^2} \qquad \text{(Eq. 12)}$$
$$FWHM_{post} = 0.9410\mu m$$

Thus, we conservatively estimate the extent of sidewall printing to be on the order of 1 μm.

Estimating Energy of Neutrophil-FN Interaction

If cell wetting (i.e. FN ligation of cell surface receptors) alone drives the spherical-to-sessile drop shape change than the energy of this interaction must be sufficient to deform the resisting cortical tension of quiescent neutrophils. The following is an order of magnitude analysis to estimate the available binding energy of human neutrophils. The total MAC-1 availability of activated human neutrophils is on the order of ~ 10^5 receptors (9). Our antibody

blocking experiments demonstrated that β_2 integrins were a major mediator of neutrophil-FN binding. From kinetic studies of β_2 integrin ligation, the energy liberated upon binding is known to be on the order of ~ -10 k_BT (10). Assuming all MAC-1 is available for binding and FN binding sites are in excess of MAC-1 than an upper estimate on the liberated binding energy ($\gamma_{cell\text{-}FN}$) is on the order of ~ -10^6 k_BT. Assuming surface energy alone dictates cell shape we can apply Young's equation to relate the observed contact angle of the cell profile to the energy of cell-substrate interaction (Eq. 13):

$$0 = \gamma_{cell-FN} + \gamma_{cell-PBS} * \cos\theta \qquad \text{(Eq. 13)}$$

Note in Eq. 13 we implicitly assumed that the energy of substrate-aqueous (i.e. FN-PBS) interaction is insignificant ($\gamma_{FN\text{-}PBS}$ ~ 0). Rearranging Eq. 13 and solving for the surface energy of the quiescent neutrophil ($\gamma_{cell\text{-}PBS}$) yields (Eq. 14):

$$\gamma_{cell-PBS} = \frac{-\gamma_{cell-FN}}{\cos\theta} \qquad \text{(Eq. 14)}$$

From z-stacks of fluorescently labeled neutrophils on FN we can measure the contact angle that the cell forms with the substrate. Contact angles from neutrophils on flat PDMS (Fig. 5 *A v*), microcontact printed with large continuous fields of FN, were used as this case represents the maximum binding energy available to the cell. For flat PDMS, $\theta = 15 \pm 2$ ° (m ± sd, n = 6 cells). Substituting Eq. 14 for $\gamma_{cell\text{-}FN}$ ~ -10^6 k_BT and $\theta = 15$ ° yields $\gamma_{ceSll\text{-}PBS} > 10^6$ k_BT. The surface energy of the quiescent neutrophil is the cortical tension (T_{cort}) multiplied by the surface area SA (Eq. 15):

$$\gamma_{cell-PBS} = T_{cort} * SA \qquad \text{(Eq. 15)}$$

Modeling the spread neutrophil as a hemispherical cap and computing the lateral surface area yields SA = 446 ± 56 μm^2. Substituting $\gamma_{cell\text{-}PBS}$ ~ 10^3 pN·μm (1 k_BT ~ 0.004114 pN·μm) and SA = 446 μm^2 into Eq. 15 yields T_{cort} ~ 10 pN/μm which is within one order of magnitude of the measured cortical tension of quiescent neutrophils (10). Our rough analysis suggests that the upper bound of available energy of the cell-FN interaction on flat PDMS is on the order of the surface energy associated with the resting neutrophil's cortical tension. However, the actual binding energy is likely lower on the discretized adhesive environment of the printed post arrays.

Furthermore, if the energy of cell-substrate binding alone were sufficient to explain the deformation we would have expected that reducing cortical tension and decreasing viscosity via cytochalasin B treatment would have increased the spreading velocity of neutrophils as was observed of cytochalasin D treated HeLa cells by Cuvelier et al (11). However, in the cytochalasin B case neutrophils spread slower than untreated control cells.

Supporting Material

Henry et al. Protrusive and Contractile Forces of Spreading Human Neutrophils

Movie Captions

Movie S1. Spreading neutrophil corresponding to Fig. 1 *B*. (*Left*) Brightfield channel. (*Right*) DiI labeled posts in fluorescence channel. Displacement vectors are enlarged 5X to aid visualization.

Movie S2. Jasplakinolide cortical stiffening abrogates neutrophil spreading. (*Left*) The evolution of surface processes, visible in the brightfield channel, suggest the cell senses the presence of FN but is incapable of translating the signal into mechanical spreading. Surface processes were not observed in control experiments. (*Right*) No post deflections above the background noise were observed in the fluorescence channel.

Supporting Material

Henry et al. Protrusive and Contractile Forces of Spreading Human Neutrophils

Supporting References

1. Desai, R. A., M. K. Khan, S. B. Gopal, and C. S. Chen. 2011. Subcellular spatial segregation of integrin subtypes by patterned multicomponent surfaces. *Integr Biol* 3:560-567.
2. Beer, F. P., E. R. Johnston, and J. T. DeWolf. 2006. *Mechanics of Materials*. McGraw-Hill Higher Education, Boston.
3. Yang, M. T., J. Fu, Y. K. Wang, R. A. Desai, and C. S. Chen. 2011. Assaying stem cell mechanobiology on microfabricated elastomeric substrates with geometrically modulated rigidity. *Nat Protoc* 6:187-213.
4. Schoen, I., W. Hu, E. Klotzsch, and V. Vogel. 2010. Probing cellular traction forces by micropillar arrays: contribution of substrate warping to pillar deflection. *Nano Lett* 10:1823-1830.
5. Lemmon, C. A., N. J. Sniadecki, S. A. Ruiz, J. L. Tan, L. H. Romer, and C. S. Chen. 2005. Shear force at the cell-matrix interface: enhanced analysis for microfabricated post array detectors. *Mech Chem Biosyst* 2:1-16.
6. Ghibaudo, M., A. Saez, L. Trichet, A. Xayaphoummine, J. Browaeys, P. Silberzan, A. Buguin, and B. Ladoux. 2008. Traction forces and rigidity sensing regulate cell functions. *Soft Matter* 4:1836-1843.
7. Schindelin, J., I. Arganda-Carreras, E. Frise, V. Kaynig, M. Longair, T. Pietzsch, S. Preibisch, C. Rueden, S. Saalfeld, B. Schmid, J. Y. Tinevez, D. J. White, V. Hartenstein, K. Eliceiri, P. Tomancak, and A. Cardona. 2012. Fiji: an open-source platform for biological-image analysis. *Nat Methods* 9:676-682.
8. Hecht, E. 1998. *Optics*. Addison-Wesley, Reading, Mass.
9. Diamond, M. S., and T. A. Springer. 1993. A subpopulation of Mac-1 (CD11b/CD18) molecules mediates neutrophil adhesion to ICAM-1 and fibrinogen. *J Cell Biol* 120:545-556.
10. Krasik, E. F., K. E. Caputo, and D. A. Hammer. 2008. Adhesive dynamics simulation of neutrophil arrest with stochastic activation. *Biophys J* 95:1716-1728.
11. Cuvelier, D., M. Thery, Y. S. Chu, S. Dufour, J. P. Thiery, M. Bornens, P. Nassoy, and L. Mahadevan. 2007. The universal dynamics of cell spreading. *Curr Biol* 17:694-699.